New Journal of Physics
The open access journal at the forefront of physics
Deutsche Physikalische Gesellschaft DPG IOP Institute of Physics

PAPER • OPEN ACCESS

Valley controlled spin-transfer torque in ferromagnetic graphene junctions

To cite this article: Zhi Ping Niu 2018 *New J. Phys.* **20** 103021

New Journal of Physics
The open access journal at the forefront of physics

Deutsche Physikalische Gesellschaft DPG
IOP Institute of Physics

Published in partnership with: Deutsche Physikalische Gesellschaft and the Institute of Physics

CrossMark

OPEN ACCESS

RECEIVED
29 June 2018

REVISED
9 September 2018

ACCEPTED FOR PUBLICATION
28 September 2018

PUBLISHED
15 October 2018

PAPER

Valley controlled spin-transfer torque in ferromagnetic graphene junctions

Zhi Ping Niu
College of Science, Nanjing University of Aeronautics and Astronautics, Jiangsu 210016, People's Republic of China
E-mail: zpniu@nuaa.edu.cn

Keywords: spin-transfer torque, valleytronics, graphene

Abstract

The presence of the valley degree of freedom in graphene leads to the valleytronics, in which information is encoded by the valley quantum number of the electron. We propose a valley controlled spin-transfer torque (STT) in graphene-based normal/normal/ferromagnetic junctions with the normal lead irradiated by the off-resonant circularly polarized light. The interplay of the spin–orbit interaction and the staggered potential in the central normal part results in the coupling between the valley and spin degrees of freedom, so a valley dependent spin polarized current can be demonstrated, which can exert a valley controlled STT on the ferromagnetic lead. The amplitude of the STT can be manipulated by the intensity of the light, the Fermi energy and the magnetization direction of the ferromagnetic lead. This valley controlled STT may find potential application in future valleytronics and spintronics.

1. Introduction

Over the past decade, motivated by the development of spintronics, the presence of the valley degree of freedom in graphene leads to the valleytronics [1, 2], whose goal is to manipulate the valley degree of freedom and search for its potential applications in semiconductor technologies and quantum information. Much substantial progress in valleytronics has been made recently, such as quantum valley Hall effect [3–6], valley polarization controlled by circularly polarized light in molybdenum disulfide [7], and valley and spin currents in silicene junctions [8–10]. Interestingly, if the intrinsic spin–orbit interaction and the staggered potential coexist in graphene-like materials, the band structure becomes spin-valley coupling, so one can control the spin polarized current by the valley degree of freedom [8–11].

Recently, on the other hand, the spin-transfer torque (STT) has also attracted much attention [12–19]. When a spin polarized current is injected into a ferromagnetic layer with a magnetization misaligned to the spin polarization of the current, it can transfer spin angular momentum to the ferromagnetic layer, and hence exerts a torque on the magnetic moments of the ferromagnetic layer, which may change the magnetization orientation of the ferromagnetic layer. The STT effect has the potential application in random access memory, which offers an all-electrical read and write process. The STT was theoretically predicted by Slonczewski [12] and Berger [13], and then it has been extensively confirmed experimentally [14]. Recently, the STT in ferromagnetic graphene junctions has also been reported. Yokoyama and Linder [15] demonstrated that both the magnitude and the sign of the STT can be controlled by means of the gate voltage in a bulk ferromagnetic/normal/ferromagnetic graphene junction. Then Ding *et al* [16] investigated theoretically the effect of strain on the STT in a zigzag-edged graphene nanoribbon spin-valve device. Later Zhang *et al* [17] studied the helical spin polarized current induced STT in graphene-based normal/topological insulator/ferromagnetic junctions. Although the STT in ferromagnetic graphene junctions has been investigated in [15–17], the effect of the valley degree of freedom on the STT is not explored. If the coupling between the valley and spin degrees of freedom exists, a valley controlled spin polarized current is generated. Naturally, it is interesting to discuss the effect of the valley degree of freedom on the STT in a ferromagnetic graphene junction.

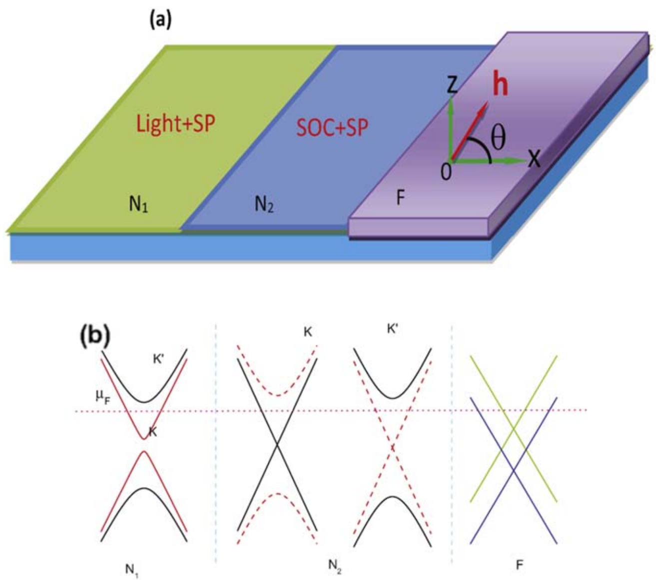

Figure 1. (a) Schematic plot of a $N_1/N_2/F$ junction, where a graphene monolayer sheet in the *xy* plane is grown on the substrates. Here the staggered potential induced by the substrates is assumed to be finite in the N_1 and N_2 but zero in the F. (b) The band structure of the $N_1/N_2/F$ junctions. In the N_1, the spin is degenerate, and due to the interaction between the staggered potential (SP) and the light, a valley dependent band gap exists. In the N_2, the interplay of the spin–orbit interaction (SOC) and the SP leads to the coupling between the valley and spin degrees of freedom. While in the F the valley is degenerate.

In this work, we predict a valley controlled STT in graphene-based normal/normal/ferromagnetic ($N_1/N_2/F$) junctions, where the N_1 is irradiated by the off-resonant circularly polarized light. In the N_1, the valley polarization can be modulated by the interaction between the staggered potential and the light. While in the N_2, the interplay of the spin–orbit interaction and the staggered potential leads to the coupling between the valley and spin degrees of freedom. In this case one can control the valley dependent spin polarized current by the valley degree of freedom, so a valley controlled STT is demonstrated. The influences of the intensity of the light, the Fermi level and Rashba spin–orbit interaction on the STT are discussed.

The rest of this paper is organized as follows. In section 2 we give the Hamiltonian of the $N_1/N_2/F$ junctions, discretize the Hamiltonian in the basis $|x_i\rangle \otimes |k_y\rangle$, and then present the formula of the valley dependent STT by the Keldysh non-equilibrium Green's function method. In section 3, numerical results and detailed discussions are demonstrated. Finally, in section 4 we summarize the main conclusions of this work.

2. Model and formulation

We consider a graphene-based two dimensional $N_1/N_2/F$ junction (see figure 1(a)) with the interfaces located at $x = 0$ and $x = L$, where L is the width of the N_2. The N_1 ($x < 0$) is irradiated by off-resonant circularly polarized light that requires $\hbar\omega \gg \gamma$ in principle, where ω is the frequency of light and γ is the nearest-neighboring hopping energy in graphene [20–24]. In the central part N_2 the spin–orbit interaction and the staggered potential are considered, which leads to the coupling between the valley and spin degrees of freedom. The ferromagnetic electrode deposited on top of the graphene sheet ($x > L$) induces a finite exchange field $\mathbf{h} = h(\cos\theta,\ 0,\ \sin\theta)$ [8, 15, 25], where h is the magnitude of exchange field and θ describes the direction angle of the magnetization. In the low-energy approximation, the Hamiltonian of the present junctions is expressed as [8, 9, 21, 26]

$$H^{\eta\sigma} = \sigma_0 \otimes [\hbar v_F(\eta k_x\tau_x + k_y\tau_y) + (\eta\lambda_\omega - \lambda_v)\tau_z] + \eta\lambda_{so}\sigma_z \otimes \tau_z - \sigma\cdot\mathbf{h} \otimes \tau_0. \tag{1}$$

Here $\eta = +1(-1)$ represents the $K\,(K')$ valley with v_F the velocity of electrons. τ_j and σ_j ($j = x, y, z, 0$) are the Pauli matrices and unit matrices in valley and spin space, respectively. $\eta\lambda_{so}\sigma_z \otimes \tau_z$ is intrinsic spin–orbit coupling term in graphene. As indicated in Kane and Mele investigation [26], graphene will be driven into topological phase when this term in graphene is enhanced. In general, the spin–orbit interaction is very weak in graphene. However, many works suggested that spin–orbit interaction can be enhanced by the substrates or adatom deposition [27–30], which results in the nontrivial topological phase. λ_ω is related to the intensity of the off-resonant circularly polarized light and provides an additional site energy of a sublattice in the N_1. By using the Floquet theory [20–24] λ_ω can be written as $\lambda_\omega = 8\pi\alpha\xi I v_F^2/\omega^3$, where $\xi = +(-)$ corresponds to the right-hand (left-hand) circularly polarized light with the frequency ω, the intensity I, and the fine structure constant

$\alpha \simeq 1/137$. The sign and strength of λ_ω can be tuned by the handedness and the intensity of the circularly polarized light. It is noted that for the system under the off-resonant circularly polarized light, light does not directly excite electrons but effectively modifies the electron band structures through virtual photon absorption processes [31]. In this case the systems would not heat up by the light. λ_v is the staggered potential induced by the substrates [32, 33], which is assumed to be finite in the N_1 and N_2 but zero in the F. By solving equation (1), the dispersion relation of the N_1 for the electrons can be written as

$$\varepsilon_{\eta\sigma}^{n} = n\sqrt{(\lambda_v - \eta\lambda_\omega)^2 + (\hbar v_F k)^2}, \tag{2}$$

where $n = +(-)$ represents the conduction (valence) band, and $k = \sqrt{k_x^2 + k_y^2}$ is the modulus of wave vector $\vec{k} = (k_x, k_y)$. It is noted that for the electrons in the η valley there exists an energy gap $E_g^\eta = 2|\lambda_v - \eta\lambda_\omega|$, which can be tuned by the parameters λ_v and λ_ω. The energy ε of the incident electron should be satisfy $|\varepsilon| > E_g^\eta/2$ to generate propagating incident modes in the η valley of the normal lead.

Due to the translation invariant along the y-axis, the transversal wave vector k_y of the incident electron must be conserved. Following the [34], we can discretize the Hamiltonian (1) in the basis $\{|x_i\rangle \otimes |k_y\rangle\}$ as,

$$H_{i,i'}^{\eta\sigma} = H_{i,i}\delta_{i',i} - \mathrm{i}E_0\sigma_0 \otimes \tau_x\delta_{i',i+1} + \mathrm{i}E_0\sigma_0 \otimes \tau_x\delta_{i',i-1}, \tag{3}$$

where $E_0 = \frac{\hbar v_F}{2a}$ and $a = x_{i+1} - x_i$ with $a = 0.5$ nm [35] is the mesh spacing along the x direction ($i \leqslant 0$ for the left lead, $1 \leqslant i \leqslant N$ for the central part, and $i \geqslant N + 1$ for the right lead). $H_{i,i}$ is given as

$$H_{i,i} = \sigma_0 \otimes [\hbar v_F k_y \tau_y + (\eta\lambda_\omega - \lambda_v)\tau_z] + \eta\lambda_{\mathrm{so}}\sigma_z \otimes \tau_z - \sigma \cdot \mathbf{h} \otimes \tau_0. \tag{4}$$

The valley dependent STT are studied by the non-equilibrium Green's function method. The influence of the two semi-infinite leads can be treated by using the iteration technique [36–38]. The retard Green's function of the central part N_2 can be calculated by the following expression:

$$G^r(\varepsilon) = \left[(\varepsilon + \mathrm{i}\eta)I - H_C - \sum\nolimits_L^r - \sum\nolimits_R^r\right]^{-1}, \tag{5}$$

where the self-energy is $\sum_{L(R)}^r = H_{CL(R)} g_{L(R)}^r H_{L(R)C}$ with $g_{L(R)}^r$ the surface retarded Green's function of the left (right) lead [36–38]. $H_{CL(R)}$ ($H_{L(R)C}$) is the coupling matrix between the left (right) lead and the central part, and H_C is the Hamiltonian of the N_2. For a small bias voltage, the valley dependent STT per unit of the bias voltage in zero temperature can be obtained as

$$\tau_\eta^{Rx} = \frac{e}{4\pi}\sum_{k_y} Tr[(G^r(\mu_F)\Gamma_L(\mu_F)G^{r+}(\mu_F)\Gamma_R(\mu_F))(\sigma_x\cos\theta - \sigma_z\sin\theta)], \tag{6}$$

where μ_F is the Fermi level. By using equation (6), we can obtain the total STT $\tau^{Rx} = \tau_K^{Rx} + \tau_{K'}^{Rx}$.

3. Results and discussions

Before presenting the numerical results for the valley dependent STT in the $N_1/N_2/F$ junctions, we first make a physical analysis for the valley dependent STT. As shown in equation (2), in the N_1 the spin is degenerate and the valley polarization can be manipulated by stagger potential and the off-resonant circularly polarized light. While from equation (1) the dispersion relation of the N_2 can be written as $\varepsilon_{\eta\sigma}^n = n\sqrt{(\lambda_v - \eta\sigma\lambda_{so})^2 + (\hbar v_F k)^2}$, where $n = +(-)$ corresponds to the conduction (valence) band. Therefore, the interplay of the spin–orbit interaction λ_{so} and the stagger potential λ_v in the N_2 leads to the coupling between the valley and spin degrees of freedom. When the electrons travel across the N_2, the currents become spin polarized and have different spin polarization in the K and K' valleys, so the torques for the K and K' valleys exerted on the F may have different amplitude and sign.

In what follows we show some numerical results for the valley dependent STT in the $N_1/N_2/F$ junctions. Figure 2(a) shows the valley dependent STT as a function of the magnetization direction of the F. Here the light is not considered, so that due to the valley degeneracy in the N_1, the current injected into the junction from the N_1 is valley unpolarized. As seen in figure 1(b), the solid (dashed) lines in the N_2 correspond to the spin-up (spin-down) channel. When the electrons travel across the N_2, only spin-up (spin-down) electrons in the K (K') valley can arrive at the N_2/F interface (see figure 1(b)), so the torques for the K and K' valleys have opposite sign. As seen in figure 2(a), τ_K^{Rx} and $\tau_{K'}^{Rx}$ (in units of $\frac{eWE}{4\pi\hbar v_F}$ with W the width of the junction and $E = 1$ meV) are periodic functions of θ with the period of 2π. However, because of the presence of the relationship of $\tau_{K(K')}^{Rx}(\theta) = \tau_{K'(K)}^{Rx}(\theta + \pi)$, the period of τ^{Rx}, which is the sum of τ_K^{Rx} and $\tau_{K'}^{Rx}$, is π. τ_K^{Rx} and $\tau_{K'}^{Rx}$ have opposite sign, so compared with τ_K^{Rx} and $\tau_{K'}^{Rx}$, τ^{Rx} is significantly reduced. In order to enhance τ^{Rx}, valley polarization in the N_1 is needed, where the incident current for one valley increases but it for the other valley decreases. In figure 2(b), the effect of the light on τ^{Rx} is discussed. When λ_ω is finite, because the relationship of $\tau_{K(K')}^{Rx}(\theta) = \tau_{K'(K)}^{Rx}(\theta + \pi)$ is absent, the period of τ^{Rx} becomes 2π instead of π. With increase of λ_ω the

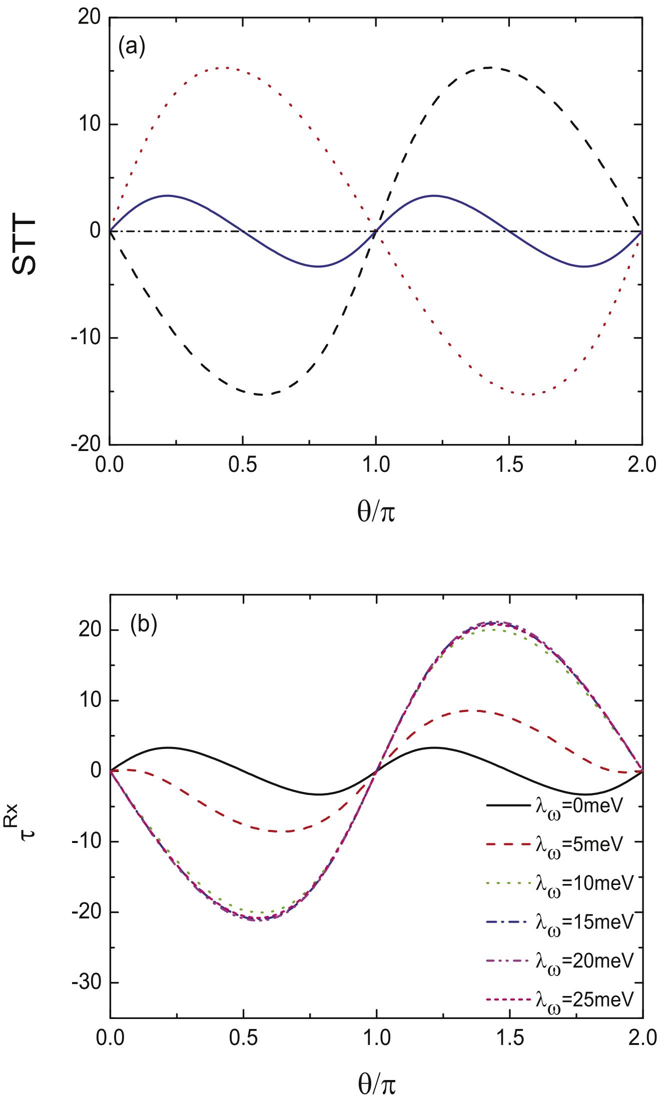

Figure 2. (a) τ_K^{Rx} (dashed line), $\tau_{K'}^{Rx}$ (dotted line) and τ^{Rx} (solid line) versus θ at $\lambda\omega = 0$. (b) τ^{Rx} versus θ at different $\lambda\omega$. Here the other parameters are taken as $L = 100$ nm, $\lambda = 0$ meV, $\mu_F = 30$ meV, $\lambda_v = 20$ meV and $h = 20$ meV.

amplitude of τ^{Rx} first increases and then begins to decrease, so in order to get a large τ^{Rx}, one should choose an appropriate parameter λ_ω. We can understand this behavior as follows. For a finite positive λ_ω, because the density of states of the incident electrons in the K valley nonmonotonically depends on λ_ω, the current coming from the K valley first increases and then decreases with λ_ω, leading to a nonmonotonic dependence of τ_K^{Rx} on λ_ω. While for the parameters taken here the density of states of the incident electrons in the K' valley monotonically decreases with λ_ω and becomes zero for large λ_ω, so $\tau_{K'}^{Rx}$ decreases and becomes zero for large λ_ω.

As discussed above, the off-resonant circularly polarized light strongly influences on the valley dependent STT, so it is interesting to analyze the effect of λ_ω on the valley dependent STT in detail. Figure 3(a) displays the valley dependent STT as a function of λ_ω at $\theta = \pi/4$ (black lines), $\pi/2$ (read lines) and $3\pi/4$ (blue lines). As shown in equation (2), the band structure of the η valley in the N_1 has an band gap E_g^η, which can be tuned by λ_ω. For the K valley $\mu_F > E_g^K/2$ should be satisfied to generate propagating incident modes in the N_1, so for the parameters $\mu_F = 30$ meV and $\lambda_\omega = 20$ meV taken here, τ_K^{Rx} nonmonotonically depends on λ_ω in the regime of -10 meV $< \lambda_\omega < 50$ meV. On the other hand, for the K' valley $\mu_F > E_g^{K'}/2$ is needed to generate propagating incident modes, thus $\tau_{K'}^{Rx}$ nonmonotonically depends on λ_ω in the regime of -50 meV $< \lambda_\omega < 10$ meV. In this case the curves of τ_x versus λ_ω can divide into three regimes. (1), For -50 meV $< \lambda_\omega < -10$ meV τ^{Rx} is positive and only originates from $\tau_{K'}^{Rx}$. (2), For -10 meV $< \lambda_\omega < 10$ meV both τ_K^{Rx} and $\tau_{K'}^{Rx}$ contribute to τ^{Rx}, which changes from positive to negative with increase of λ_ω. (3), For $\lambda_\omega > 10$ meV τ^{Rx} is negative and only comes from τ_K^{Rx}. At $\theta = \pi/2$, due to the presence of $\tau_{K'}^{Rx}(\lambda_\omega) = \tau_K^{Rx}(-\lambda_\omega)$, τ^{Rx} is an odd function of λ_ω (red dotted line in figure 3(a)). On the other hand, for the other θ, the symmetry of $\tau_{K'}^{Rx}(\lambda_\omega) = \tau_K^{Rx}(-\lambda_\omega)$ is broken, τ^{Rx} is not an odd function of λ_ω any more. In order to explain the behavior of τ_η^{Rx}, we divide τ_η^{Rx} into two parts:

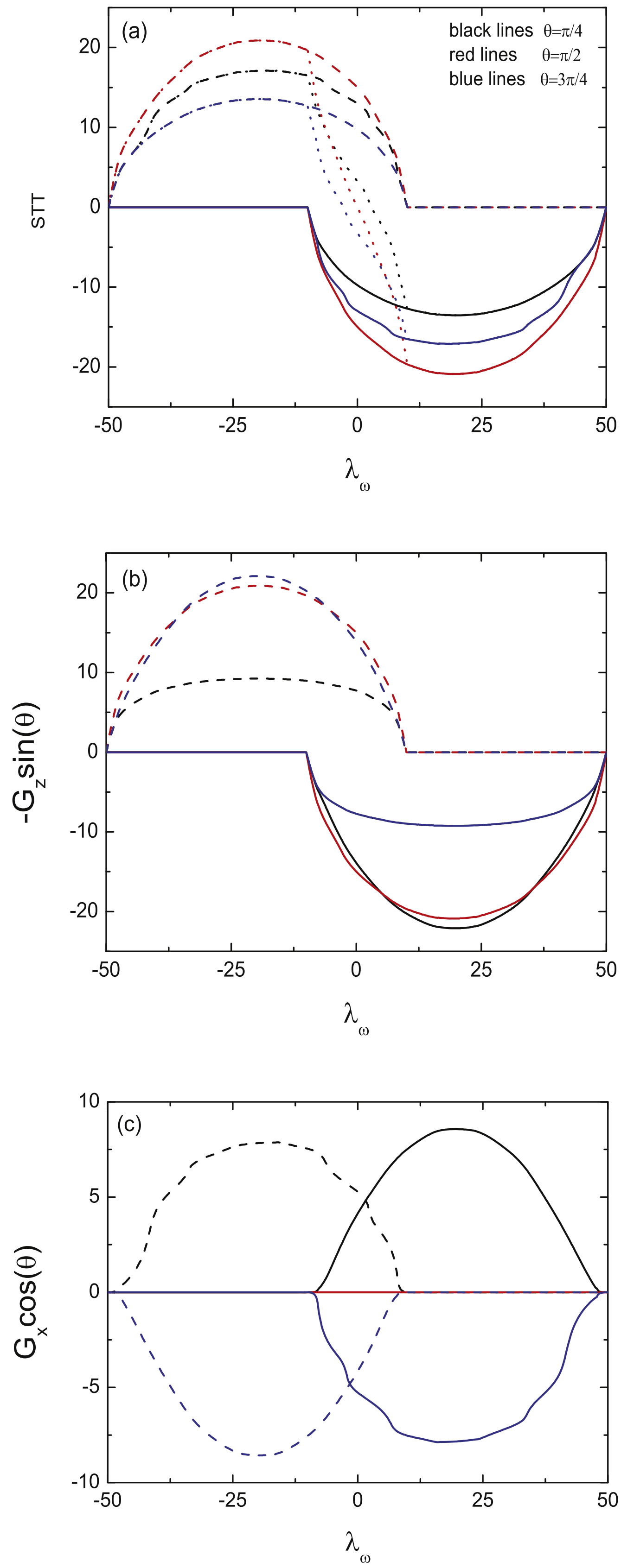

Figure 3. (a) τ_K^{Rx} (solid lines), $\tau_{K'}^{Rx}$ (dashed lines) and τ^{Rx} (dotted lines) versus λ_ω at different θ. (b) $-G_z \sin\theta$ and (c) $G_x \cos\theta$ versus λ_ω at different θ. Other parameters are the same as those in figure 2.

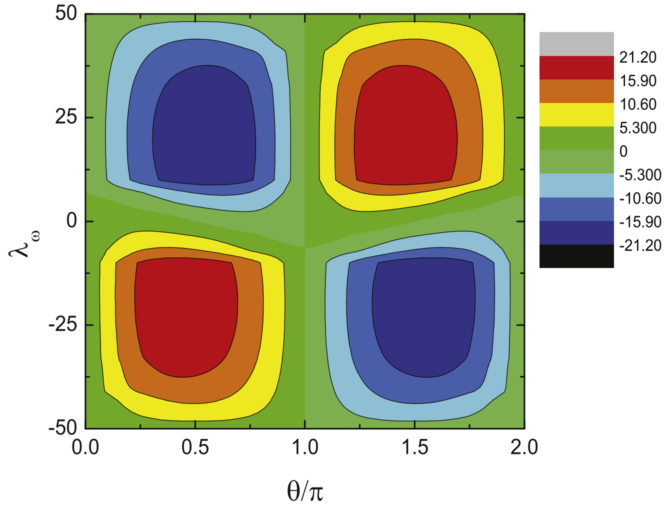

Figure 4. τ^{Rx} as a function of the spin–orbit interaction λ_{so} and the angle θ of the magnetization direction of the F. Other parameters are the same as those in figure 2.

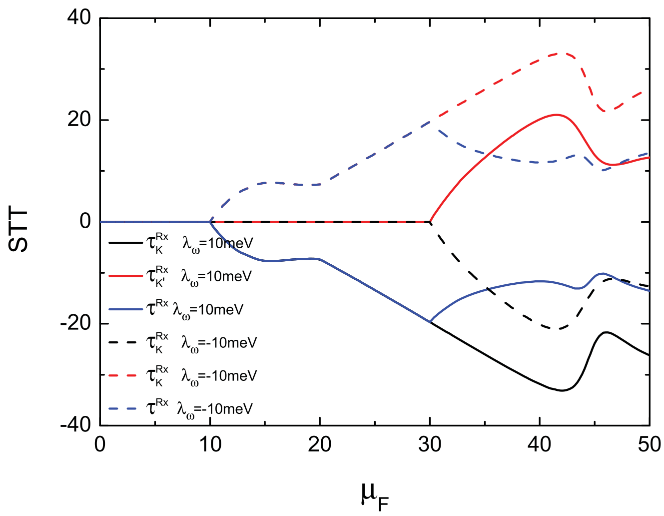

Figure 5. τ_K^{Rx}, $\tau_{K'}^{Rx}$ and τ^{Rx} versus μ_F. Other parameters are the same as those in figure 2.

$\tau_{\eta 1}^{Rx} = -G_z \sin\theta$ and $\tau_{\eta 2}^{Rx} = G_x \cos\theta$ with $G_{z(x)} = \frac{e}{4\pi}\sum_{k_y} Tr(G^r \Gamma_L G^{r+} \Gamma_R \sigma_{z(x)})$. For $\theta = \pi/2$ $\tau_{\eta 2}^{Rx}$ is zero and τ_η^{Rx} only comes from $\tau_{\eta 1}^{Rx}$, which has the symmetry of $\tau_{K'1}^{Rx}(-\lambda_\omega) = \tau_{K1}^{Rx}(\lambda_\omega)$, thus τ^{Rx} is an odd function of λ_ω. However, for $\theta = \pi/4$ or $3\pi/4$ both τ_{K1}^{Rx} and τ_{K2}^{Rx} ($\tau_{K'1}^{Rx}$ and $\tau_{K'2}^{Rx}$) are finite and contribute to τ_K^{Rx} ($\tau_{K'}^{Rx}$). τ_{K1}^{Rx} and $\tau_{K'1}^{Rx}$ have the opposite sign (figure 3(b)), but τ_{K2}^{Rx} and $\tau_{K'2}^{Rx}$ have the same sign (figure 3(c)). Because τ_η^{Rx} comes from the combined contribution of $\tau_{\eta 1}^{Rx}$ and $\tau_{\eta 2}^{Rx}$, which breaks the symmetry of $\tau_{K'}^{Rx}(\lambda_\omega) = \tau_K^{Rx}(-\lambda_\omega)$, τ^{Rx} is not an odd function of λ_ω any more.

Since the STT strongly depends on the magnetization direction of the F (figure 2) and the off-resonant circularly polarized light (figure 3), the STT as a function of θ and λ_ω is plotted in figure 4. It is found that the STT is zero for $\theta = 0, \pi, 2\pi$, where the spin polarization direction of the incident current is parallel or antiparallel to the magnetization direction of the F. For θ is near the angles $\theta = \frac{\pi}{2}, \frac{3\pi}{2}$ the STT can reach maximum. When θ is fixed, as discussed in figure 2, with increase of λ_ω the amplitude of τ^{Rx} first increases and then begins to decrease, so in order to get a large τ^{Rx}, one should choose an appropriate parameter λ_ω. We also find by changing the sign of λ_ω, the STT can convert from the negative to positive, so we can control the STT direction by the handedness of the light.

Furthermore, let us discuss the effect of the Fermi level μ_F on the valley dependent STT at $\lambda_\omega = 10$ meV (solid lines) and -10 meV (dashed lines) in figure 5. At $\lambda_\omega = 10$ meV τ^{Rx} is finite and negative for $\mu_F > 10$ meV. With increase of μ_F τ^{Rx} (blue solid line) first increases with its slope changing at $\mu_F = 15$ and

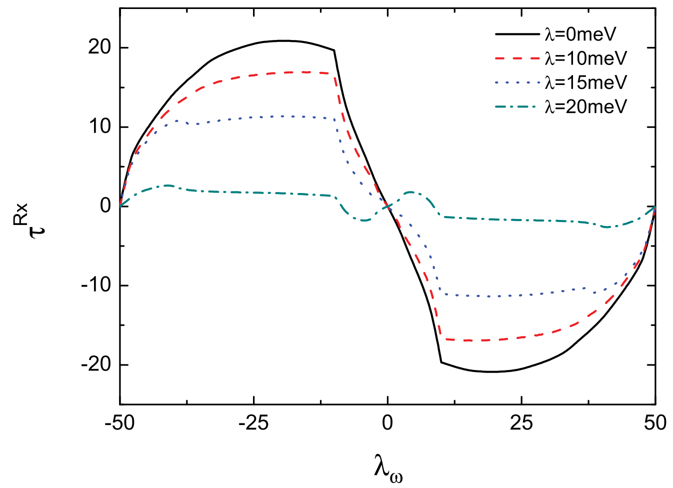

Figure 6. τ^{Rx} versus λ_ω with different λ. Other parameters are the same as those in figure 2.

20 meV, and then decreases for $\mu_F > 30$ meV. This can be explained by τ_K^{Rx} (black solid line) and $\tau_{K'}^{Rx}$ (red solid line). When μ_F is smaller than 10 meV, because μ_F lies in the band gap of the K valley in the N_1, the current is zero, leading to vanishing τ_K^{Rx}. For 10 meV $< \mu_F <$ 20 meV μ_F locates at the conduction band of the K valley in the N_1, the current becomes finite. We find a finite τ_K^{Rx}, whose amplitude first increases and then becomes almost constant for 15 meV $< \mu_F <$ 20 meV. This is because in this regime τ_K^{Rx} depends on the density of states of the band structure $E_{R+} = \pm(\hbar v_F k + h)$ and $E_{R-} = \pm(\hbar v_F k - h)$ in the right F, which, respectively, decreases and increases with μ_F, so τ_K^{Rx} first increases and then becomes almost constant for 15 meV $< \mu_F <$ 20 meV. For $\mu_F >$ 20 meV the density of states of E_{R+} (E_{R-}) increases with μ_F, so the spin polarized current exerted on the F increases, leading to the increase of τ_K^{Rx}. Once μ_F is larger than 30 meV, μ_F also locates at the conduction band of the K' valley in the N_1, $\tau_{K'}^{Rx}$ increases with μ_F. Because τ_K^{Rx} and $\tau_{K'}^{Rx}$ have opposite sign, τ^{Rx} relies on the competition of τ_K^{Rx} and $\tau_{K'}^{Rx}$. $\tau_{K'}^{Rx}$ increases faster than τ_K^{Rx}, so with further increasing of μ_F the amplitude of τ_x decreases. Due to the presence of the relationship of $\tau_{K(K')}^{Rx}|_{\lambda_\omega=10\text{ meV}} = -\tau_{K'(K)}^{Rx}|_{\lambda_\omega=-10\text{ meV}}$, one observes the STTs at $\lambda_\omega = -10$ meV and $\lambda_\omega = 10$ meV have the same amplitude but opposite sign, thus the sign of the STT can be controlled by handedness of the light.

In addition, due to the presence of the structure inversion asymmetry in the z direction, the Rashba spin–orbit interaction $\lambda(\sigma_x \otimes \tau_y - \eta\sigma_y \otimes \tau_x)$ may appear in the N_2. In figure 6 we study the effect of the Rashba spin–orbit interaction on τ^{Rx} at $\theta = \pi/2$. As shown in figure 6 τ^{Rx} is an odd function of λ_ω and decreases with λ. This is because without λ the current can arrive at the N_2/F interface with the spin polarization direction along z (for the K valley) or $-z$ (for the K' valley) axis, which is perpendicular to the magnetization direction of the F. However, when λ is finite, the electrons precess in the process of traveling across the N_2, so the spin polarization direction deviates from the z axis, which results in the decrease of τ^{Rx} with λ. Therefore in order to obtain a large τ^{Rx}, a small λ is needed.

Last we will comment on the experimental feasibility of our results. The staggered potential can be induced by the substrate. Actually, in experiment, the gap induced by the SiC substrate can range from several meV to 0.26 eV [32, 33]. A strong spin–orbit interaction can be induced by the substrates or adatom deposition [27–30]. For example, Kou *et al* reported a large intrinsic spin–orbit interaction is generated in Bi_2Se_3/graphene/Bi_2Se_3 [28] or BiTeI/graphene/BiTeI [29] quantum well structure. In the N_2 we can consider a Bi_2Se_3/graphene/SiC or BiTeI/graphene/SiC quantum well structure, where the staggered potential and spin–orbit interaction are induced by the proximity effect, respectively. In fact, we can also use silicene or stanene as a central part, which has strong intrinsic spin–orbit interaction but weak Rashba spin–orbit interaction. The off-resonant circularly polarized light requires $\hbar\omega \gg \gamma$ in principle, so the frequency should be larger than 3500 THz [20]. When one takes the lowest frequency of light, $\omega \approx 3500$ THz, and $|\lambda_\omega| \approx 0.0026$–0.39 eV [20] is obtained when graphene is irradiated by an ultrashort pulse [39] with the range of laser intensity from 10^{10} to 1.5×10^{12} W cm^{-2}. Here the spin is degenerate in the normal lead, the spin polarization of the current originates from the spin-valley coupling in the central part, so a large central region width L is needed. For large L ($L > 50$ nm), the contribution of evanescent states to the currents is completely suppressed, and τ^{Rx} is nearly independent of L (not shown here). A real N_1/N_2/F junction also inevitably contains impurities or atomic defects in the bulk. As pointed in [40, 41], to realize the valley controlled STT, the defect ratio cannot exceed 8%, otherwise the valley controlled STT effect is broken by defect states. It should be pointed out that the amplitude of τ^{Rx} obtained here is comparable to the STT in a previous work, where a ferromagnetic/normal/ferromagnetic junction is investigated [15]. However, unlike [15], the spin polarized currents in this work originates from the coupling between the valley and spin degrees of freedom, so the STT reported here does not require additional ferromagnetic layer with fixed magnetization.

4. Summary

In summary, we study the valley dependent STT in $N_1/N_2/F$ junctions. The N_1 is irradiated by the off-resonant circularly polarized light, and the valley polarization can be modulated by the interaction between the staggered potential and the light. While in the N_2, due to the interplay of the spin–orbit interaction and the staggered potential induced by the substrate, the band structure is spin-valley coupling, so one can control the valley dependent spin polarized current by the valley degree of freedom, which exerts a valley controlled STT on the F. The effects of the intensity of the light, the Fermi level and Rashba spin–orbit interaction on the STT are investigated. The valley controlled STT reported here suggests the ferromagnetic graphene junction ideal for very efficient magnetization manipulation of magnetic materials without external magnetics fields.

Acknowledgments

This work was supported by the National Natural Science Foundation of China under Grant No. 11374158.

References

[1] Rycerz A, Tworzydlo J and Beenakker C W J 2007 *Nat. Phys.* **3** 172
[2] Schaibley J R, Yu H, Clark G, Rivera P, Ross J S, Seyler K L, Yao W and Xu X 2016 *Nat. Rev. Mater.* **1** 16055
[3] Xiao D, Yao W and Niu Q 2007 *Phys. Rev. Lett.* **99** 236809
[4] Gorbachev R V, Song J C W, Yu G L, Kretinin A V, Withers F, Cao Y, Mishchenko A, Grigorieva I V, Novoselov K S, Levitov L S and Geim A K 2014 *Science* **346** 448
[5] Ju L *et al* 2015 *Nature* **520** 650
Shimazaki Y, Yamamoto M, Borzenets I V, Watanabe K, Taniguchi T and Tarucha S 2015 *Nat. Phys.* **11** 1032
Sui M *et al* 2015 *Nat. Phys.* **11** 1027
[6] Niu Z P and Yao J 2018 *Phys. Lett.* A **382** 920
[7] Mak K F, He K, Shan J and Heinz T F 2012 *Nat. Nanotechnol.* **7** 494
Zeng H, Dai J, Yao W, Xiao D and Cui X 2012 *Nat. Nanotechnol.* **7** 490
[8] Niu Z P and Dong S 2014 *Appl. Phys. Lett.* **104** 202401
[9] Niu Z P, Zhang Y M and Dong S 2015 *New. J. Phys.* **17** 073026
[10] Zhai X, Wang Y-T, Wen R, Wang S-X, Tian Y, Zhou X, Chen W and Yang Z 2018 *Phys. Rev.* B **97** 085410
[11] Yokoyama T 2013 *Phys. Rev.* B **87** 241409(R)
Tsai W-F, Huang C-Y, Chang T-R, Lin H, Jeng H-T and Bansil A 2013 *Nat. Commun.* **4** 1500
Yamakage A, Ezawa M, Tanaka Y and Nagaosa N 2013 *Phys. Rev.* B **88** 085322
[12] Slonczewski J C 1996 *J. Magn. Magn. Mater.* **159** L1
[13] Berger L 1996 *Phys. Rev.* B **54** 9353
[14] Miron I M, Garello K, Gaudin G, Zermatten P-J, Costache M V, Auffret S, Bandiera S, Rodmacq B, Schuhl A and Gambardella P 2011 *Nature* **476** 189
Liu L, Lee O J, Gudmundsen T J, Ralph D C and Buhrman R A 2012 *Phys. Rev. Lett.* **109** 096602
Mellnik A R *et al* 2014 *Nature* **511** 449
[15] Yokoyama T and Linder J 2011 *Phys. Rev.* B **83** 081418(R)
[16] Ding K-H, Zhu Z-G and Su G 2014 *Phys. Rev.* B **89** 195443
[17] Zhang Q, Chan K S and Li J 2018 *Sci. Rep.* **8** 4343
[18] Ralph D C and Stiles M D 2008 *J. Magn. Magn. Mater.* **320** 1190
[19] Brataas A, Kent A D and Ohno H 2012 *Nat. Mater.* **11** 372
[20] Zhou X, Xu Y and Jin G 2015 *Phys. Rev.* B **92** 235436
[21] Ezawa M 2013 *Phys. Rev. Lett.* **110** 026603
[22] Zhai X and Jin G 2014 *Phys. Rev.* B **89** 235416
[23] Yan Z and Wang Z 2016 *Phys. Rev. Lett.* **117** 087402
Zhang X-X, Ong T and Nagaosa N 2016 *Phys. Rev.* B **94** 235137
Niu Z P and Wu X 2018 *Phys. Lett.* A **382** 729
Niu Z P and Dong S 2015 *Europhys. Lett.* **111** 37007
[24] Wang J, Yang Y H and Chan K S 2014 *Phys. Rev.* B **89** 064501
[25] Haugen H, Hernando D H and Brataas A 2008 *Phys. Rev.* B **77** 115406
[26] Kane C L and Mele E J 2005 *Phys. Rev. Lett.* **95** 226801
[27] Weeks C, Hu J, Alicea J, Franz M and Wu R 2011 *Phys. Rev.* X **1** 021001
Jin K and Jhi S 2013 *Phys. Rev.* B **87** 075442
[28] Kou L, Yan B, Hu F, Wu S, Wehling T O, Felser C, Chen C and Frauenheim T 2013 *Nano Lett.* **13** 6251
[29] Kou L, Wu S, Felser C, Frauenheim T, Chen C and Yan B 2014 *ACS Nano* **8** 10448
[30] Hu F M, Kou L and Frauenheim T 2015 *Sci. Rep.* **5** 8943
[31] Kitagawa T, Oka T, Brataas A, Fu L and Demler E 2011 *Phys. Rev.* B **84** 235108
Bukov M, D'Alessio L and Polkovnikov A 2015 *Adv. Phys.* **64** 139
Sheremet A S, Kibis O V, Kavokin A V and Shelykh I A 2016 *Phys. Rev.* B **93** 165307

[32] Zhou S Y, Gweon G-H, Fedorov A V, First P N, de Heer W A, Lee D-H, Guinea F, Castro Neto A H and Lanzara A 2007 *Nat. Mater.* **6** 770
[33] Rotenberg E, Bostwick A, Ohta T, McChesney J L, Seyller T and Horn K 2008 *Nat. Mater.* **7** 258
[34] Nam Do V, Hung Nguyen V, Dollfus P and Bournel A 2008 *J. Appl. Phys.* **104** 063708
[35] Xu G J, Wu B H and Cao J C 2011 *J. Appl. Phys.* **109** 083704
[36] Lopez Sancho M P, Lopez Sancho J M and Rubio J 1984 *J. Phys. F: Met. Phys.* **14** 1205
[37] Liang Q and Dong J 2008 *Nanotechnology* **19** 355706
[38] Niu Z P and Xing D Y 2010 *Eur. Phys. J.* B **73** 139
Niu Z P 2011 *J. Phys.: Condens. Matter* **23** 435302
Niu Z P and Xing D Y 2012 *Appl. Phys. Lett.* **101** 062601
[39] Roberts A, Cormode D, Reynolds C, Newhouse-Illige T, LeRoy B J and Sandhu A S 2011 *Appl. Phys. Lett.* **99** 051912
[40] Zhai X, Zhang S, Zhao Y, Zhang X and Yang Z 2016 *Appl. Phys. Lett.* **109** 122404
[41] Zhai X, Wang S and Zhang Y 2017 *New J. Phys.* **19** 063007